Catalysis Today 155 (2010) 92–100

Contents lists available at ScienceDirect

Catalysis Today

journal homepage: www.elsevier.com/locate/cattod

Comparison of ceramic honeycomb monolith and foam as Ni catalyst carrier for methane autothermal reforming

Paolo Ciambelli *, Vincenzo Palma, Emma Palo

Dipartimento di Ingegneria Chimica e Alimentare, Università degli Studi di Salerno, Via Ponte Don Melillo 84084 Fisciano (Salerno), Italy

ARTICLE INFO

Article history:
Available online 23 February 2009

Keywords:
Autothermal reforming
Structured catalysts
Washcoating
Monolith
Foam

ABSTRACT

Structured ceramic honeycomb monolith and open cell foams were employed as Ni catalyst carrier for methane autothermal reforming (CH_4-ATR). The catalysts were prepared through washcoating of the supports with a commercial CeO_2–Al_2O_3-based slurry and further impregnation into aqueous solution of nickel acetate tetrahydrate. A quite good reproducible preparation procedure was individuated in terms of both washcoat loading and resistance to ultrasonic vibrations and thermal shock tests. The catalysts were characterized by means of several techniques such as XRD, SEM, N_2 adsorption at −196 °C, Hg porosimetry and H_2-TPR. The catalytic activity towards CH_4-ATR was tested in kW-scale autothermal reforming reactor which is able to produce up to 5 m^3(stp)/h of H_2. The reactor is thermally integrated with two heat exchangers for the preheating of the air and liquid water fed to the system, thus being completely self-sustained and able to perform without any external heat source. The tests carried out aiming to evaluate the influence of the O_2/CH_4 ratio on catalytic performance showed the higher activity of foam structured samples which can provide a lower average temperature in the catalytic bed.

1. Introduction

Structured reactors have been successfully used in numerous applications ranging from the treatment of automotive exhaust gases to chemical and refining applications. The advantages of monolithic or foam reactors over conventional packed bed reactors include high geometric surface area, low pressure drop when associated with high flow rates, efficient mass transfer, high thermal and mechanical stability [1]. The choice of the substrate material is a function of the operating conditions adopted in the specific application. In particular, the well recognized use of cordierite is due to its unique combination of several critical characteristics such as high melting point and excellent thermal shock resistance, high porosity and pore size distribution suitable for ease of washcoat application and good washcoat adherence [2]. Indeed, owing to cordierite low specific surface area, in order to increase the surface area it is necessary to use a washcoat of an inorganic oxide acting as a host for the active species. The washcoat layer is usually applied onto the structured substrate by impregnation of this one by a powder slurry and subsequent calcination. Very often, more than one impregnation is required to load the substrate with the necessary amount of washcoat. The final objective of the deposition process is to load the substrate with the desired amount of washcoat, in the form of a uniform, homogeneous layer with a minimum number of impregnations [3]. Thus, several studies performed to optimize the washcoating technique suggest that the washcoat characteristics of homogeneity, reproducibility and adhesion are affected by the slurry solid content, particle size, viscosity, pH and drying temperature [4–7].

Over the last years, the short contact time reactors, based on monoliths and foams, have been considered as promising systems for the production of synthesis gas [8–12], particularly in small scale applications (hydrogen fuelling stations, on-board reformers or fuel cell-based combined heat and power units) in which the accommodation of high throughputs and reduced reactor volume is required.

The conventional route for hydrogen production from hydrocarbons is the steam reforming process where the kinetics, and therefore the throughput, is limited by the rate at which the heat generated in external burners can be transferred to the catalytic bed where the endothermic reforming reactions take place [13]. Thus, hydrogen production using autothermal reforming (ATR) has recently attracted considerable attention due to its high energy efficiency with low investment cost due to its simple system design. Since in ATR the heat for the reforming reactions is supplied by internal combustion, there is no need to supply heat to the reactor over and above the amount provided in the preheating of

* Corresponding author. Tel.: +39 089964151; fax: +39 089964057.
E-mail address: pciambelli@unisa.it (P. Ciambelli).

0920-5861/$ – see front matter © 2009 Elsevier B.V. All rights reserved.
doi:10.1016/j.cattod.2009.01.021

the reactants. The overall chemical reactions taking place in the ATR include partial oxidation, steam reforming, and water gas shift. The main advantages deriving from the use of the autothermal reforming process are related to economics of scale, since much larger single-stream units are possible with adiabatic ATR than with steam reforming, and the size of equipment is smaller, because ATRs are very compact units compared to steam reformers [14].

Catalysts formulation for ATR depends on the fuel choice and operating temperature. However, generally, it should possess some peculiar characteristics such as resistance to intermittent operations and cycles, particularly on start-up and shut-down, resistance to sulphur and coke formation, especially in the catalytic zone that runs oxygen limited [15].

Although nowadays precious metals are preferred in reforming reactions [16–18], the use of Ni-based catalysts is still a challenge and an attractive option due to their relatively high activity and low cost. Indeed, recently, some studies were carried out dealing with the development of Ni-based catalysts supported on ceramic monoliths for the autothermal reforming of isooctane [19] and dodecane [20,21] aiming to elucidate the effect of the drying procedure on Ni distribution and the effect of the presence of a cerium–zirconium oxide on the catalyst deactivation and carbon deposition resistance.

In this study the first objective was to individuate an optimized and reproducible procedure for the preparation of ceramic Ni-based catalysts, structured in the form of monolith and foam to be employed in methane autothermal reforming reaction for hydrogen production. The second objective was to test the activity of the prepared catalysts evaluating and discussing their performance in terms of hydrogen yield and temperature profile along the catalytic bed in a kW-scale self-sustained ATR reactor.

2. Experimental

2.1. Catalyst preparation

The washcoating procedure was developed with 400 cpsi cordierite monoliths and 65 ppi α-alumina-based foams (Vesuvius Hi Tech Ceramics). Series of five specimens of monoliths and foams were prepared in order to check the reproducibility of the results according to a well-known procedure described in the review of Avila et al. [22]. The procedure was carried out on pretreated and unpretreated supports in order to verify the influence of this step on washcoat adhesion. The calcination pre-treatment was carried out in air at 1000 °C for 1 h with a dT/dt equal respectively to 16 °C/min for monolith samples and 2 °C/min for foams.

The supports were further dipped vertically for 10 min into a commercial slurry (ECOCAT), CeO_2–Al_2O_3-based (28.5 wt% solids content after calcination in air at 1000 °C for 1 h, pH of about 3.9), then withdrawn at a controlled speed [7] and the excess of slurry was evacuated through aspiration. The supports were dried at 120 °C for 24 h and weighted. The procedure was repeated three times. Finally, the washcoated supports were calcined in air at 1000 °C for 1 h (dT/dt = 16 °C/min). The washcoat layer thickness was geometrically calculated. The washcoated supports were further dipped into an aqueous solution of 0.8 M $Ni(CH_3COO)_2{\cdot}4H_2O$ for 30 min at 100 °C to carry out the deposition of the active species. In order to check the influence of the drying procedure on the Ni adhesion, some samples were slowly dried at 100 °C for 1 h (dT/dt = 0.4 °C/min) and calcined at 1000 °C for 1 h (dT/dt = 2 °C/min), other samples were flash dried at 120 °C for 30 min and then calcined in air at 1000 °C for 1 h (dT/dt = 16 °C/min). For both cases the dip-coating procedure was repeated three times in order to obtain the desired Ni amount which has been evaluated by the sample weight increase after the deposition and expressed as NiO.

2.2. Catalyst characterization

The adhesion ability of washcoated supports was assessed at first by resistance to ultrasonic vibrations and then by resistance to thermal shock. Ultrasonic adhesion tests were carried out according to the method described in the literature [23]. The coated supports were immersed in petroleum ether inside a sealed beaker and then treated in an ultrasonic bath (CEIA CP104) for 1–30 min (for monoliths) and 1–50 min (for foams) to measure the weight loss caused by exposure to ultrasonication. The thermal shock tests were carried out introducing the samples in an oven at 1000 °C and kept for 3 min at this temperature. Then they were quenched at room temperature. The procedure was repeated six times monitoring the weight change after each cycle. The weight loss was defined as follows:

$$\Delta W\,(\%) = \frac{W_{be\,fore} - W_{a\,fter}}{W_{be\,fore}} \times 100$$

where W_{before} and W_{after} are respectively the washcoat weight before and after ultrasonic vibration or thermal shock tests.

The crystalline phases present in the catalysts were determined by X-ray diffraction (XRD) analysis, carried out with a Bruker D8 diffractometer using Cu Kα radiation in the range 20–80° 2θ. The data were compared to reference data from the International Centre for Diffraction Data (ICDD).

The surface morphology of samples was examined by the LEO 420 scanning electron microscope (SEM) on pieces cut from monoliths or foams. The imaging was performed after metallization of the samples with Au film.

The textural characterization was performed with a Sorptometer Kelvin 1040 (Costech Instruments) by using N_2 adsorption at −196 °C and the BET method for the evaluation of specific surface area. The samples were outgassed in He flow at 150 °C for 30 min before adsorption measurements. Moreover, the foams were characterized in terms of pore size distribution by Hg porosimetry with PASCAL 240 and 440 apparatuses.

The catalysts reducibility in the presence of hydrogen was studied by thermogravimetric analysis (TGA-H_2) with a TA Instruments Q600 thermobalance in a 5% H_2/He flow (100 cm^3(stp)/min) and in the temperature range 25–1100 °C (dT/dt = 10 °C/min).

2.3. Catalytic activity tests

Catalytic activity tests were performed with a self-sustained ATR reactor (Fig. 1a and d), able to produce up to 5 m^3(stp)/h of H_2 and thermally integrated with two heat exchangers for the preheating of the fed air (Fig. 1b) and liquid water (Fig. 1c) by the hot exhaust stream, thus operating without any external heat sources [24,25].

The stainless steel ATR reactor (i.d. 36 mm), which has been successfully operated with structured noble metals-based catalysts at high gas hourly space velocities up to 90,000 h^{-1} [26,27], consists of: (i) a lower section where, only during the start-up phase, does methane react with air at a fixed O_2/CH_4 ratio and (ii) an upper catalytic section where reforming reactions occur in the presence of a catalyst supported by a metallic gauze. In the start-up phase the heat released in the lower section is transferred to the reforming section heating the catalytic bed up to the ATR catalyst threshold temperature. The proper mixing of the methane and air, fed at the bottom, is carried out in a chamber at the top of which a SiC foam is placed to obtain a well distributed and homogeneous flame. The inlet of water is placed at the bottom of the metallic gauze. A thermocouple is placed on the SiC foam (T comb), while three thermocouples (T_L, T_M, T_H), located respectively at 25, 50 and 75% of the catalytic bed height, provide the temperature profile in the reactor's axial

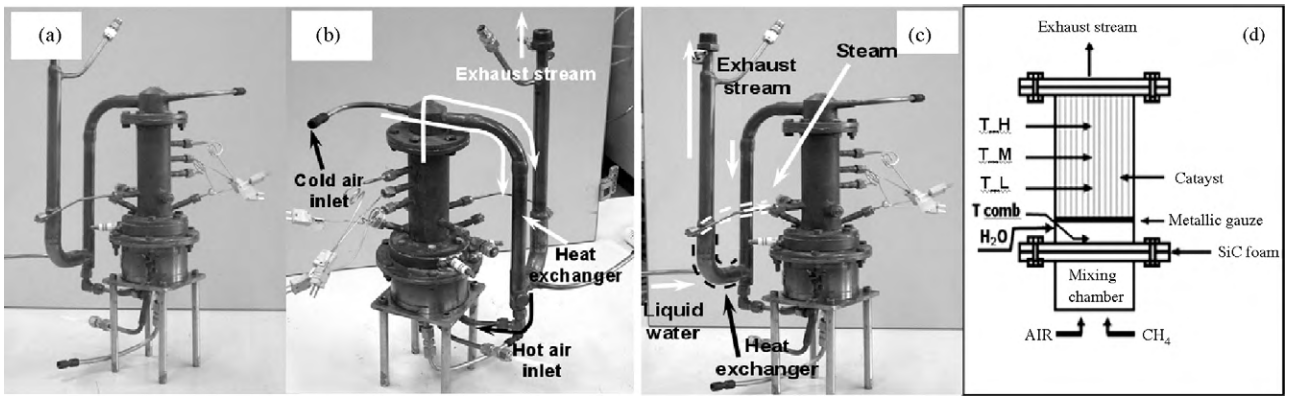

Fig. 1. Autothermal reforming reactor (a), air preheating (b), liquid water preheating (c), and reactor schematic drawing (d).

direction. A differential pressure sensor monitors the pressure drops across the reactor. The outside shell of the reactor is thermally insulated to reduce heat loss. The thermal self-sustainment of the reactor is improved by the presence of two heat exchangers to preheat the air and the water by the hot exhaust stream. Reactor start-up is performed by feeding a water-free mixture of methane and air with a molar O_2/CH_4 ratio of 1.36 and by inducing for few seconds a voltaic arc between two spark plugs placed on the surface of the SiC foam. After that, water is fed to the reactor, the O_2/CH_4 and H_2O/CH_4 ratios are varied to the desired values and, as the homogeneous combustion is inhibited, all the reactions occur simultaneously in the catalytic bed. The reactor start-up is very fast because in less than 3 min the reactor is able to reach a stable performance. A detailed description of the start-up phase and of the performance improvement owing to the thermal integration is given elsewhere [25].

The catalytic activity tests reported in this work were carried out at fixed H_2O/CH_4 molar feed ratio equal to 0.49 by changing the O_2/CH_4 ratio from 0.56 to 0.75 at a fixed gas hourly space velocity (GHSV) of 12,300 h^{-1}. Other catalytic activity tests were carried out in order to investigate the effect of gas hourly space velocity (ranging between 12,300 and 50,000 h^{-1}) on hydrocarbon conversion and hydrogen yield, where the GHSV value is defined as the ratio between the total gaseous flow rate fed to the reactor (STP conditions) and the total catalytic bed volume.

3. Results and discussion

3.1. Catalyst preparation

The optimization of the preparation procedure involved the evaluation of the influence of support pre-treatment, the verification of the reproducibility of the washcoating procedure and the influence of drying step on the washcoat layer adhesion. Typical results are here reported for honeycomb samples. The sample precalcination results in a critical step in the preparation procedure. Indeed for both the calcined and uncalcined monoliths a washcoat loading of about 28 wt% was measured after washcoating deposition and the washcoat layer was about 60 μm for both samples. Though any remarkable difference was observed during the washcoating procedure, a dramatic different behaviour was detected during ultrasonic vibrations tests reported in Fig. 2, where it is clearly shown that the precalcination step allows a better anchored washcoat layer on the honeycomb substrate as an increase of the weight loss from 6 to 13% is registered with not precalcined supports. Indeed, the thermal pre-treatment may result in a cleaning step which provides the formation of cavities in the walls of the monolith, necessary for a good sticking of the washcoat [28].

A quite good reproducible washcoating procedure on calcined samples was found. The results, reported in Fig. 3, show that on all the specimens an average washcoat loading of 28 wt% and a washcoat layer of 60 μm are obtained.

These results are in good agreement with those reported by Jiang et al. [29], according to whom the suitable solid content in the slurry gel with pH value of 2–5 is about 30 wt% and the first loading of coating can reach 8–12 wt%.

The reproducibility of washcoating procedure as well as the adhesion ability under ultrasonications and thermal shock is reported respectively in Fig. 4a and b, where the results obtained for each specimen are included in the bars.

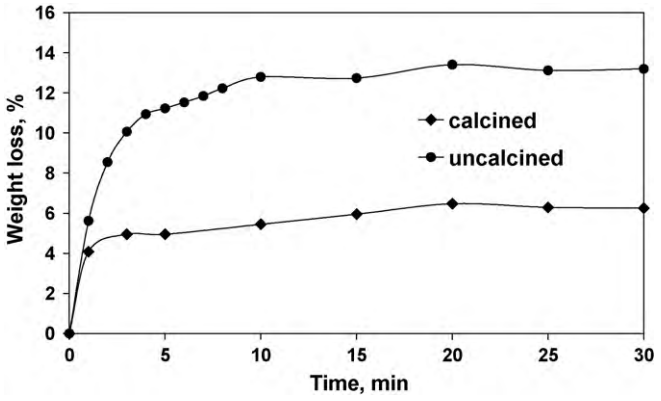

Fig. 2. Influence of precalcination step during washcoating procedure on mechanical resistance to ultrasonic vibrations.

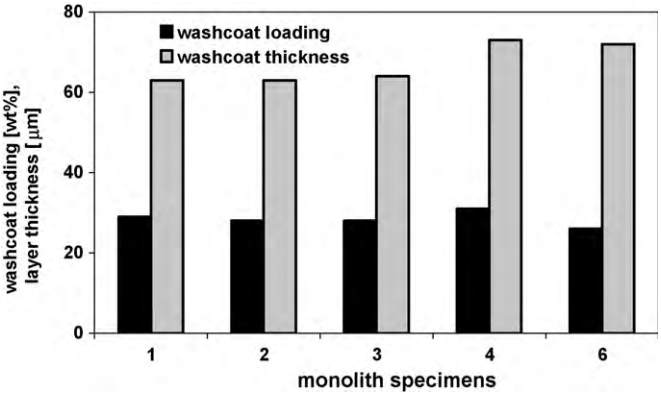

Fig. 3. Reproducibility of washcoating procedure – washcoat loading and layer thickness.

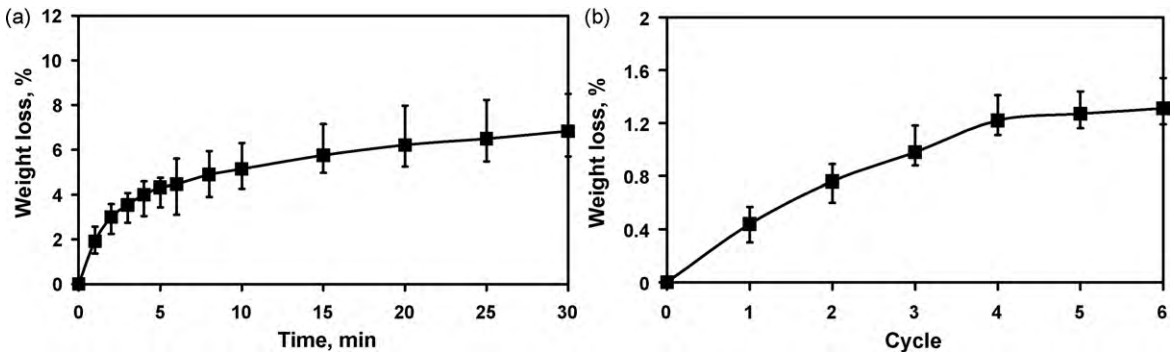

Fig. 4. Reproducibility of washcoating procedure – washcoat adhesion ability under ultrasonications (a) and thermal shock (b).

It is interesting to note that for both cases most of the losses takes place during a relatively short period in the beginning of the experiment and the weight loss curves reach a plateau soon thereafter. At the end of the experiment a weight loss of about 6 and 1.5% was observed for ultrasonic vibrations and thermal shock, respectively. The results of ultrasonic vibrations tests are consistent with those reported by Luo et al. [30]. They found a weight loss of 5.6 and 3.5% after 30 min of exposure to ultrasounds, of a CeO_2–Y_2O_3-based washcoat calcined respectively at 500 and 1200 °C. This result suggests that the high calcination temperature promotes the stability and cohesion of the washcoat. In order to evaluate the effect of drying procedure after the deposition of the active species on the washcoated support, two different samples were prepared at two different drying rates. Results of weight change during ultrasonic vibrations tests for the two monolithic samples, reported in Fig. 5, show that the drying procedure is a critical stage for the resistance of the catalyzed washcoat. Indeed the dramatic weight loss of about 3%, observed with fast drying, is significantly reduced to about 0.5% with slow drying, since high drying rate can cause abrupt water release as well as nickel acetate decomposition. This can lead to the formation of cracks which contribute to the detachment of the deposited washcoat. The importance of the drying method of wet monoliths has been also reported by Villegas et al. [19] as an inappropriate procedure can result in an uneven metal distribution, due to the complex porosity of the system (macropores of the cordierite, micro or mesopores of the washcoat), and to the particular channel structure: the solvent evaporation leads to liquid migration from the centre to the end of the channels, and to metal accumulation.

After the preparation procedure a Ni final amount of about 9 wt% was obtained for monolithic samples.

With regards to foam structured samples, in Table 1 the washcoat loading, the weight losses respectively after ultrasonications and thermal shocks, and the final Ni amount are reported. Also in this case a quite good reproducible procedure was identified, and the evaluation of washcoat layer thickness on calcined samples, obtained by SEM microscopy, gave a value of about 20 μm.

3.2. Catalyst characterization

XRD pattern obtained for washcoat calcined at 1000 °C is reported in Fig. 6. The main peaks are those relevant to the presence of CeO_2 (fluorite phase, cubic structure) at 28.5°, 33.0°, 47.5°, 56.4°, 59.4°, 69.7°, 76.5° and 79.1° (ICCD PDF No. 81-0792). Three peaks, likely due to the presence of ZrO_2, are evident at 29.8°, 50° and 59.4°. Finally, two smaller peaks at 45.8° and 67.1° are attributed to the presence of γ-Al_2O_3 [29].

The XRD patterns of monolithic samples at the different steps of preparation are reported in Fig. 7. For the Ni-based monolith,

Table 1
Foam samples preparation procedure steps.

Foam sample	Washcoat loading (wt%)	Weight loss after ultrasounds (%)	Weight loss after thermal shock (%)	Ni loading (wt%)
1	30.4	0.98	0.81	8.1
2	34.7	1.21	0.49	8.7
3	30.0	0.89	0.56	10.2
4	35.9	0.33	0.69	8.0
5	32.1	0.62	0.97	11.1

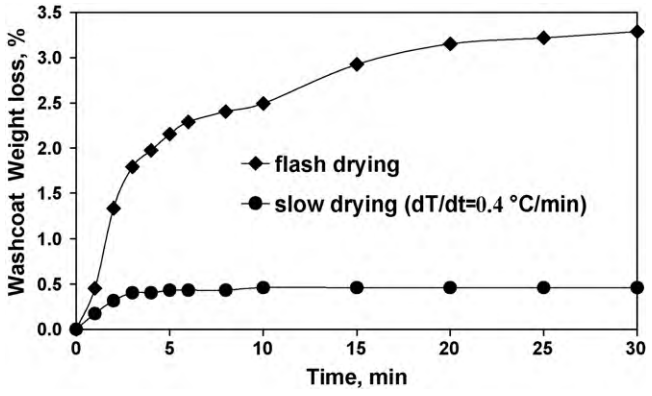

Fig. 5. Effect of drying procedure on the washcoat resistance during ultrasonic vibration test after the deposition of the active species.

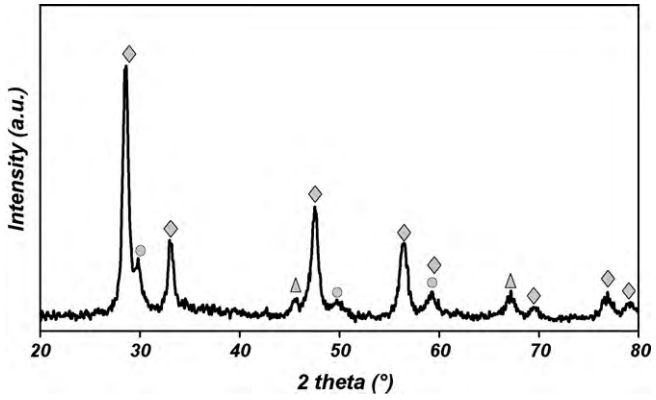

Fig. 6. XRD spectrum of washcoat calcined at 1000 °C. (◊) CeO_2, (○) ZrO_2, and (△) γ-Al_2O_3.

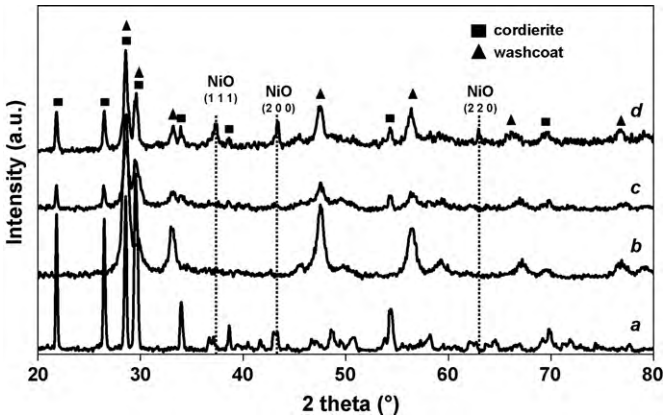

Fig. 7. XRD patterns of monolithic samples: cordierite monolith (a), washcoat (b), washcoated monolith (c), and Ni-based monolith (d).

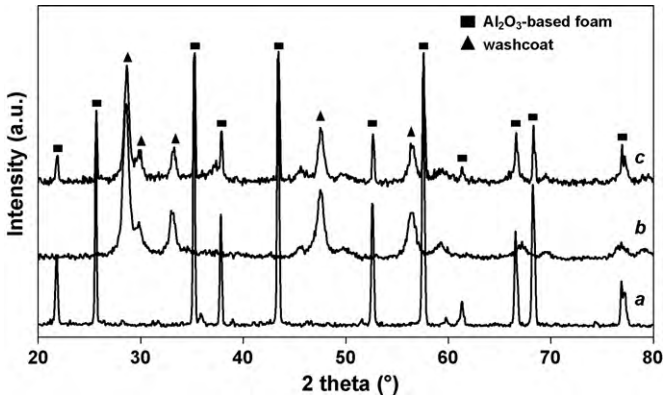

Fig. 8. XRD patterns of foam samples: Al_2O_3-based foam (a), washcoat (b), and Ni-based foam (c).

besides the peaks ascribable to the presence of cordierite like structure (ICDD PDF No. 84-1221) and washcoat, three additional peaks respectively at 37.3°, 43.4° and 62.9° are present, which can be attributed to the presence of NiO (ICDD PDF No. 78-0643).

The XRD patterns of foam samples at the different preparation steps are reported in Fig. 8. For the support the main peaks typical of α-Al_2O_3 are observed (ICDD PDF No. 42-1468). After the washcoating procedure and the Ni deposition, only the peaks due to the washcoat are detected, unlike the peaks coming from NiO. This can be due to the partial overlapping of Al_2O_3 peaks with the NiO ones [31], as well as to NiO crystallites sizes too small to be detected by XRD [32], or to the formation of well dispersed $NiAl_2O_4$. Indeed, it is reported [33] that during preparation Ni^{2+} could disperse on the surface of Al_2O_3, or diffuse into the bulk structure of Al_2O_3 to different extents transforming into $NiAl_2O_4$ spinel structure, especially during heat treatment at high temperature [33–36].

The presence of a washcoat layer homogeneously deposited on the honeycomb substrate was confirmed by SEM images reported in Fig. 9 for cordierite monolith (a), washcoated monolith (b) and after Ni deposition (c) at different magnifications.

SEM images of cordierite show an irregular structure characterized by macroporosities which can contribute to the formation of a well uniform washcoat layer (Fig. 9b). Agrafiotis et al. [6] reported that the adhesion of the washcoat layer to the support takes place primarily by a mechanism such as "anchoraging" and interlocking of the washcoat particles with the surface irregularities of the support, and to a much lesser extent via chemical or affinity mechanisms. At higher magnifications microcracks are present with an average size of 1 μm that can better contribute to the anchoring of the active species. Indeed, after Ni deposition (Fig. 9c) a more uniform layer was deposited on cordierite monoliths.

Similar results were obtained for foam samples (Fig. 10 before (a) and after washcoat and Ni deposition (b)).

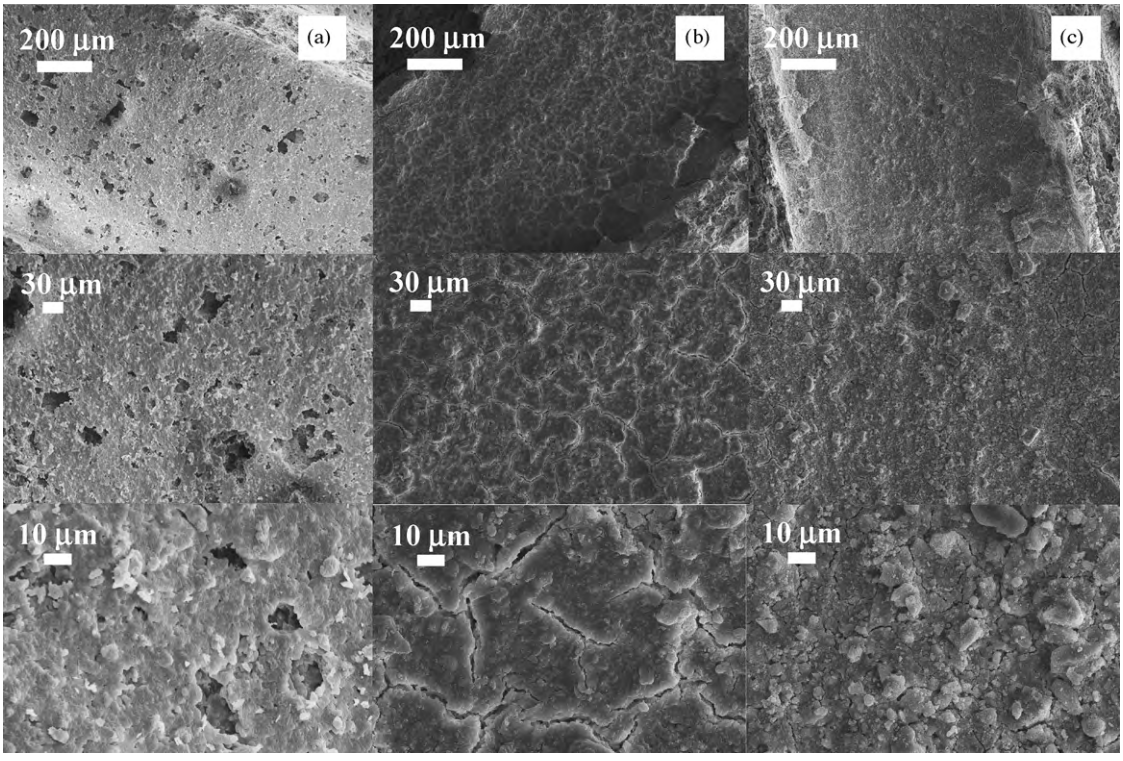

Fig. 9. SEM images for cordierite monolith (a), washcoated monolith (b) and after Ni deposition (c) at different magnifications.

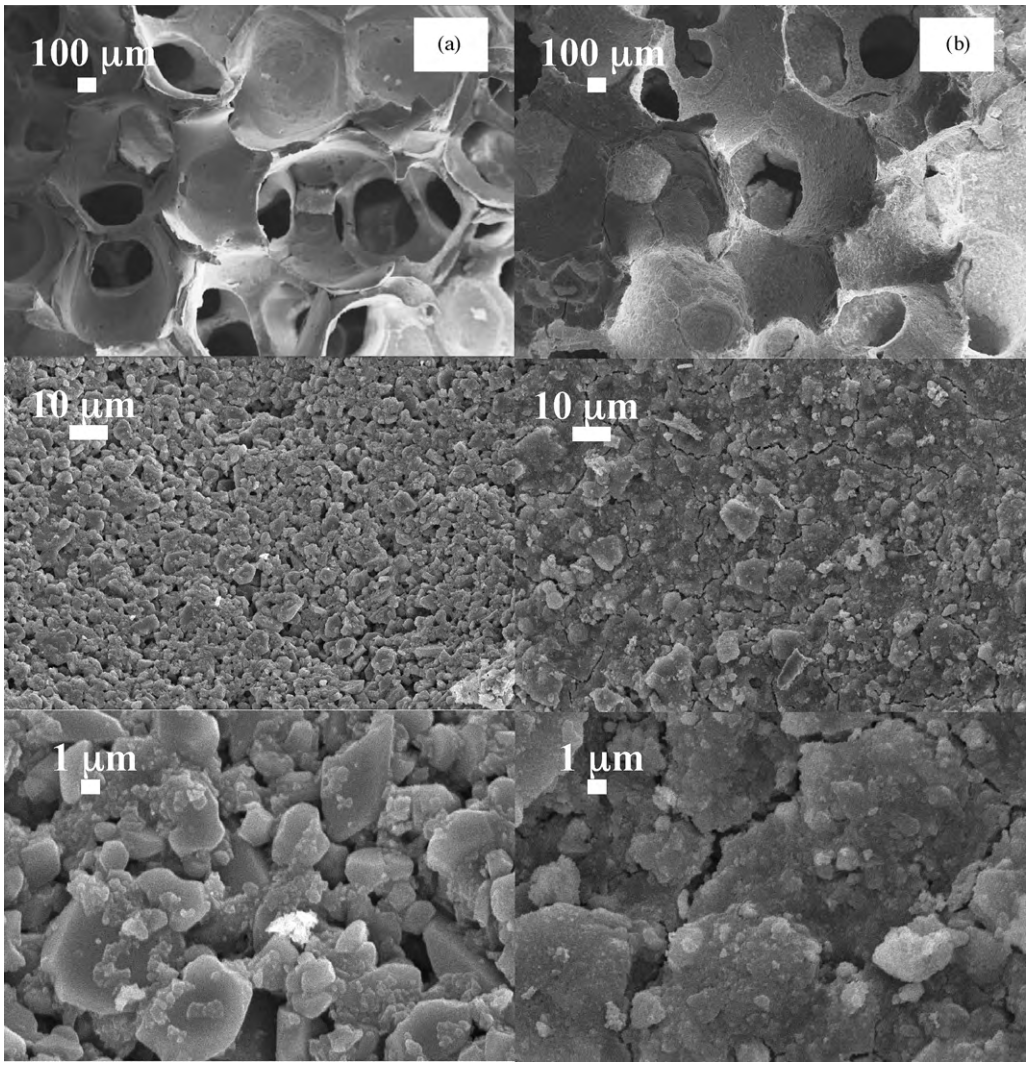

Fig. 10. SEM images of calcined foam before (a) and after washcoating and Ni deposition (b) at different magnifications.

At lower magnifications we observed the partial occlusion of foam pores after washcoating procedure. At higher magnifications a well homogeneous washcoat layer is observed with a tremendous change in the surface foam morphology; moreover, also in this case some microcracks in the washcoat are present with an average size less than 1 μm.

The textural properties of the catalysts and support are summarized in Table 2. The last column is relative to the percentage of pores in foam samples with radius ranging between 40 and 498 Å which, belonging to mesoporous range, are more interesting for catalytic activity.

Table 2
Textural properties of supports and catalysts.

Sample	B.E.T. area (m^2/g)	Cumulative porous volume (cm^3/g)	Pores r_{40-498} (%)
Washcoat	58	1.2	21.4
Cordierite monolith	2	–	–
Washcoated monolith	19	–	–
Washcoated monolith after adhesion tests	14	–	–
Ni-based monolith	6	–	–
Al_2O_3-based foam	1	0.9	0.0
Ni-based foam	15	0.7	9.2

BET specific surface area of the monolith calcined substrate was around 2 m^2/g, typical for this kind of material [37]. Its washcoating with a CeO_2–Al_2O_3-based slurry leads to an increase of the specific surface area (19.2 m^2/g) due to the porous nature of washcoat up to values in good agreement with those reported by Skoglundh et al. [38]. After adhesion tests a decrease in specific surface area was observed owing to a partial sinterization upon repeated exposure at high temperature [30]. After Ni addition and calcination at 1000 °C a further decrease of the specific surface area (6.5 m^2/g) was observed. Similar results were found for foam-based samples. Indeed, the cumulative porous volume of about 0.9 cm^3/g of alumina-based foam decreases up to about 0.7 cm^3/g of Ni-based foam since the washcoating and Ni deposition procedures can partially block the narrowest foam pores. Moreover, it must be observed that for alumina-based foam there is any contribution of pores with radius belonging to the mesoporous range. This contribution appears after washcoating and Ni deposition due to the presence of washcoat (Fig. 11).

The samples reducibility is reported in Fig. 12. The washcoat reduction profile shows two peaks, the first of which, located at about 600 °C, has very low intensity and can be attributed to reduction of the outer most layers of Ce^{4+} (surface reduction), while the following peaks at high temperature, around 925 °C, can be attributed to the reduction of the inner Ce^{4+} layer (bulk

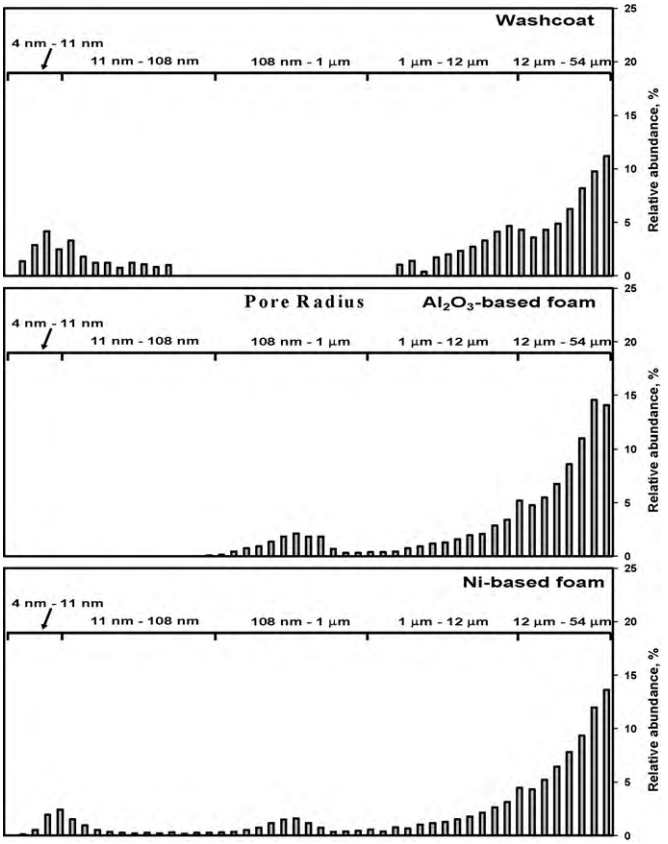

Fig. 11. Porosimetric distributions of washcoat, Al_2O_3-based foam and Ni-based foam.

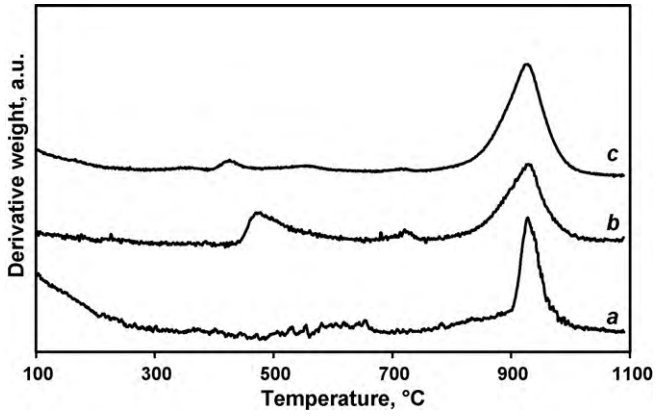

Fig. 12. H_2-TPR of washcoat (a), Ni-based monolith (b), and Ni-based foam (c).

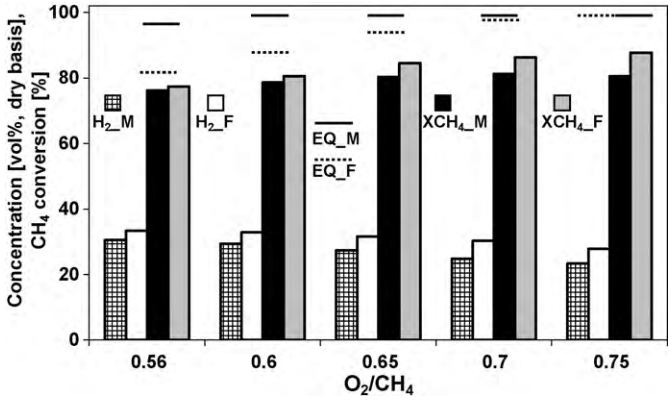

Fig. 14. Effect of O_2/CH_4 ratio on H_2 concentration and CH_4 conversion for honeycomb monolith and foam structured catalysts (H_2O/CH_4 = 0.49, GHSV = 12,300 h^{-1}).

reduction) with removal of the bulk oxygen [39,40]. However, the bulk reduction peaks is quite shifted towards higher temperature with respect to the typical values reported in the literature. As reported by Piras et al. [41], when CeO_2 is in the presence of Al_2O_3, a peak at temperature higher than 880 °C is observed, due to the reduction of Ce^{4+} beyond the thermodynamic value observed for pure ceria, which is driven by interaction with Al_2O_3 with the formation of $CeAlO_3$.

Both Ni-based catalysts reduction profiles show an additional peak at lower temperature, respectively at 470 °C for monolith sample and 425 °C for foam structured sample. Both these peaks can be attributed to the reduction of NiO. In fact, in agreement with literature data [42,43], the peak in the temperature range 400–600 °C is attributed to the reduction of Ni^{2+} in the NiO phase, according to the following reaction: $NiO \rightarrow Ni^{\delta+} \rightarrow Ni^0$. The eventual complexity of the peak may be ascribed to the presence of different NiO species [44]. However, the intensity of this reduction peak for Ni-based foam catalyst is lower and shifted towards lower temperature with respect to that of the monolith structured catalyst. Both these phenomena may be likely due to the lower crystallite size when the foam is employed as support as well as to a partial formation of $NiAl_2O_4$ species which are reduced at higher temperature of around 900 °C [37].

3.3. Catalytic activity tests

Fig. 13 shows the effect of O_2/CH_4 feed ratio on the ATR bed-temperature profile at steady state conditions for both monolith and foam structured catalysts.

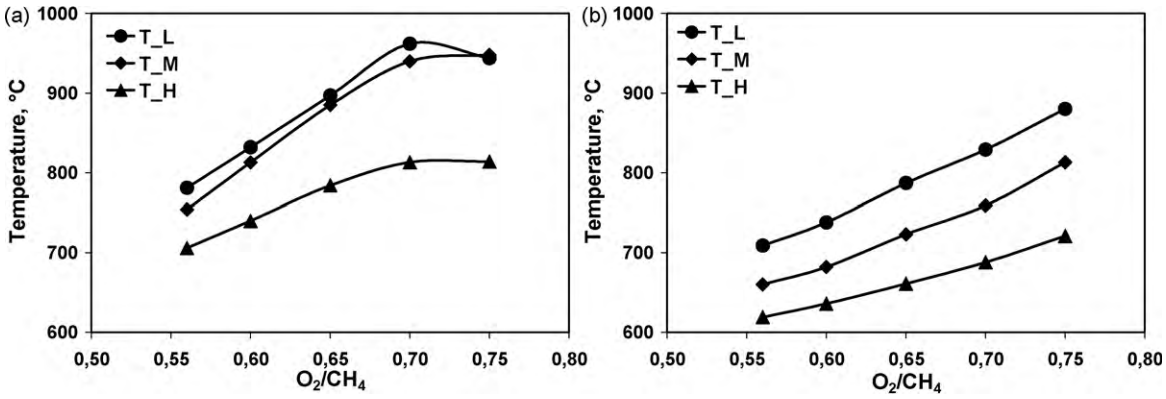

Fig. 13. Effect of O_2/CH_4 ratio on temperature profile for honeycomb (a) and foam (b) structured catalysts (H_2O/CH_4 = 0.49, GHSV = 12,300 h^{-1}).

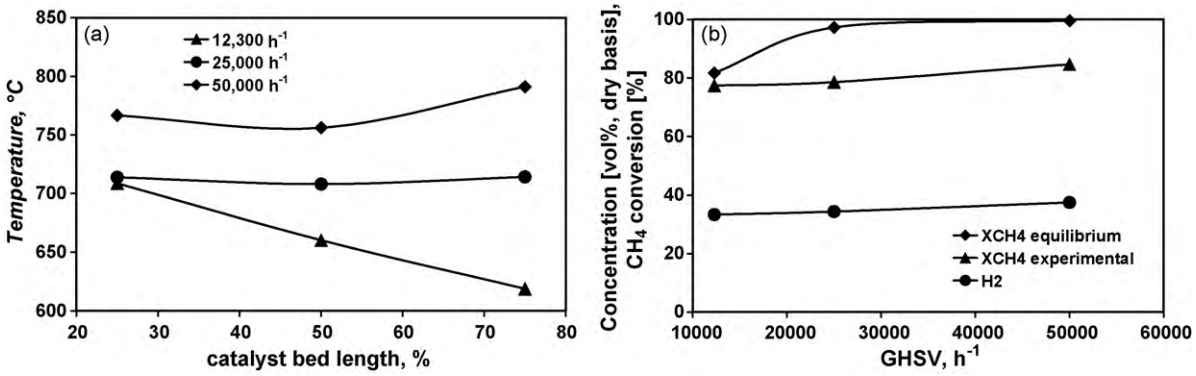

Fig. 15. Effect of space velocity on foam structured catalysts performance (O_2/CH_4 = 0.56, H_2O/CH_4 = 0.49).

Both structured catalysts have the same behaviour. At fixed O_2/CH_4 ratio the catalyst bed temperature rises at the inlet and then gradually decreases, showing the typical catalyst bed-temperature profile characteristic of an ATR reactor [44,45]. This temperature profile has been suggested to be a result of a sequential reaction mechanism involving the initial exothermic oxidation reactions of methane, followed by strongly endothermic steam reforming reactions, as well as the mildly exothermic water gas shift reaction [45–47]. At increasing O_2/CH_4 ratio, for both catalysts an increase in the average catalytic bed temperature is observed. This fact can be due to a higher occurrence of the oxidation reaction which in turn leads to an increase in the CH_4 conversion and to a decrease in reforming reaction selectivity (Fig. 14) in agreement with thermodynamic calculations [25]. Comparing the activity of both structured catalysts it is possible to observe an average lower axial temperature and a corresponding higher catalytic activity for foam catalyst at each O_2/CH_4 ratio investigated (in the plot the equilibrium conversion for both monolith and foam structured catalysts are also reported). These two phenomena may be correlated, since a higher activity towards reforming reactions leads to a higher amount of heat subtracted to oxidation reaction which in turn leads to a lower average temperature.

Generally, as reported by Horn et al. [48] when heat and mass transport limitations are controlling, such as in the catalytic partial oxidation reaction, the random porous network of a foam catalyst carrier may determine an improvement in the gas temperature profile and species diffusion, helping to realise a proper catalyst bed design. However, this effect is strictly correlated to the operating conditions [9] and to the support material nature, since a high conductivity material could minimize the occurrence of hot spots in the catalyst when highly exothermic reactions are performed [49,50].

The higher activity of foam catalyst can be related to the higher available amount of active species which is due to the higher surface to volume ratio with respect to honeycomb monolith catalyst, giving higher catalytic activity per unit reactor volume. In particular, the total amount of Ni (as NiO) for monolith and foam, are respectively 0.014 and 0.028 g/cm^3, even if the same percentage load values are realised. In addition, in the case of foam, a thinner washcoat layer is obtained (20 μm instead of 60 μm) that may be responsible for lower eventual diffusional effects.

Further investigation on the influence of space velocity on foam catalyst behaviour shows that higher GHSV values gave a flattened temperature gradient in the monitored catalytic bed zone (25–75%, Fig. 15a).

This temperature profile behaviour could be explained in terms of change in selectivity towards reforming reaction. In fact at higher space velocity, the oxidation reactions are more favoured and their high occurrence can provide for an increase in the medium and high zone of the catalyst bed. On the whole, the catalytic performance is affected by an increasing of space velocity, since the CH_4 conversion is more far from thermodynamic value (Fig. 15b). In some instance, the foam structured catalyst temperature profile can be explained also in terms of heat transfer properties. As reported by Hohn and Schmidt [51], the enhanced convective heat transfer of foams favoured the progressive cooling of the inlet portion of the bed at increasing space velocity, eventually leading to reactor blow-out. An increase in the active species amount could shift towards higher value the space velocity at which an increase in catalytic performance is observed.

4. Conclusions

A series of honeycomb and foam structured Ni catalysts were investigated in order to evaluate the effect of the support structure on the activity towards CH_4 autothermal reforming. A good reproducible preparation procedure was developed, evidencing that key parameters affecting the washcoat adhesion quality are the supports pre-treatment and the drying rate. Catalytic activity tests showed that in the range of investigated GHSV, foam structured catalysts allow a higher activity with respect to honeycomb structured catalysts as well as a lower average temperature along the catalytic bed and a more uniform temperature profile.

Acknowledgement

This work was financed by the FISR Project DM 17/12/2002 "Idrogeno puro da gas naturale mediante reforming a conversione totale ottenuta integrando reazione chimica e separazione a membrana".

References

[1] A. Cybulski, J.A. Moulijn, in: A. Cybulski, J.A. Moulijn (Eds.), Structured Catalysts and Reactors, Marcel Dekker Inc., New York, 1998.
[2] J.L. Williams, Catal. Today 69 (2001) 3.
[3] C. Agrafiotis, A. Tsetsekou, I. Leon, J. Am. Ceram. Soc. 83 (2000) 1033.
[4] C. Agrafiotis, A. Tsetsekou, J. Mater. Sci. 35 (2000) 951.
[5] C. Agrafiotis, A. Tsetsekou, J. Eur. Ceram. Soc. 20 (2000) 815.
[6] C. Agrafiotis, A. Tsetsekou, A. Ekonomakou, J. Mater. Sci. Lett. 18 (1999) 1421.
[7] M. Valentini, G. Groppi, C. Cristiani, M. Levi, E. Tronconi, P. Forzatti, Catal. Today 69 (2001) 307.
[8] A.S. Bodke, S.S. Bharadwaj, L.D. Schmidt, J. Catal. 179 (1998) 138.
[9] M. Maestri, A. Beretta, G. Groppi, E. Tronconi, P. Forzatti, Catal. Today 105 (2005) 709.
[10] B. Silberova, H.J. Venvik, A. Dolmen, Catal. Today 99 (2005) 69.
[11] I. Aartun, B. Silberova, H. Venvik, P. Pfeifer, O. Görke, K. Schubert, A. Holmen, Catal. Today 105 (2005) 469.
[12] N.J. Degenstein, R. Subramanian, L.D. Schmidt, Appl. Catal. A 305 (2006) 146.
[13] W. Balthasar, D.J. Hambleton, Int. J. Hydrogen Energy 5 (1980) 21.

[14] R.M. Navarro, M.A. Peña, J.L.G. Fierro, Chem. Rev. 107 (2007) 3952.
[15] A. Faur Ghenciu, Curr. Opin. Solid State Mater. Sci. 6 (2002) 389.
[16] A. Qi, S. Wang, C. Ni, D. Wu, Int. J. Hydrogen Energy 32 (2007) 981.
[17] B. Li, K. Maruyama, M. Nurunnabi, K. Kunimori, K. Tomishige, Appl. Catal. A 275 (2004) 157.
[18] M.M.V.M. Souza, M. Schmal, Appl. Catal. A 281 (2005) 19.
[19] L. Villegas, F. Masset, N. Guilhaume, Appl. Catal. A 320 (2007) 43.
[20] B.D. Gould, X. Chen, J.W. Schwank, J. Catal. 250 (2007) 209.
[21] B.D. Gould, X. Chen, J.W. Schwank, Appl. Catal. A 334 (2008) 277.
[22] P. Avila, M. Montes, E.E. Miró, Chem. Eng. J. 109 (2005) 11 (and references therein).
[23] S. Yasaki, Y. Yoshino, K. Ihara, K. Ohkubo, US Patent No. 5,208,206, May 4, 1993.
[24] P. Ciambelli, V. Palma, E. Palo, D. Sannino, in: Proceedings of "7th World Congress of Chemical Engineering", July 10–14, Glasgow (Scotland), 2005.
[25] E. Palo, Ph.D. Thesis, University of Salerno (Italy), 2007.
[26] G. Iaquaniello, A. Mangiapane, P. Ciambelli, V. Palma, E. Palo, Chem. Eng. Trans. 7 (2005) 261.
[27] P. Ciambelli, V. Palma, E. Palo, G. Iaquaniello, A. Mangiapane, P. Cavallero, AIDIC Conf. Ser. 8 (2007) 67.
[28] J.R. González-Velasco, M.A. Gutiérrez-Ortiz, J.L. Marc, J.A. Botas, M.P. González-Marcos, G. Blanchard, Ind. Eng. Chem. Res. 42 (2003) 311.
[29] P. Jiang, G. Lu, Y. Guo, Y. Guo, S. Zhang, X. Wang, Surf. Coat. Technol. 190 (2005) 314.
[30] M.-F. Luo, M. He, Y.-L. Xie, P. Fang, L.-Y. Jin, Appl. Catal. B 69 (2007) 213.
[31] R.M. Navarro, M.C. Álvarez-Galván, F. Rosa, J.L.G. Fierro, Appl. Catal. A 297 (2006) 60.
[32] G. Li, L. Hu, J.M. Hill, Appl. Catal. A 301 (2006) 16.
[33] B. Scheffer, P. Molhoek, J.A. Moulijn, Appl. Catal. 46 (1989) 11.
[34] P. Arnoldy, J.A. Moulijn, J. Catal. 93 (1985) 38.
[35] P.J. Mangnus, A. Bos, J.A. Moulijn, J. Catal. 146 (1994) 437.
[36] O.-S. Joo, K.-D. Jung, Bull. Korean Chem. Soc. 23 (2002) 1149.
[37] A.N. Shigapov, G.W. Graham, R.W. McCabe, M. Paputa Peck, H. Kiel Plummer Jr., Appl. Catal. A 182 (1999) 137.
[38] M. Skoglundh, H. Johansson, L. Lowendhal, K. Jansson, L. Dahl, B. Hirschauer, Appl. Catal. B 7 (1996) 299.
[39] E. Aneggi, M. Boaro, C. de Leitenburg, G. Dolcetti, A. Trovarelli, J. Alloys Compd. 408–412 (2006) 1096.
[40] M. Boaro, M. Vicario, C. de Leitenburg, G. Dolcetti, A. Trovarelli, Catal. Today 77 (2003) 407.
[41] A. Piras, S. Colussi, A. Trovarelli, V. Sergo, J. Llorca, R. Psaro, L. Sordelli, J. Phys. Chem. B 109 (2005) 11110.
[42] W. Shan, M. Luo, P. Ying, W. Shen, C. Li, Appl. Catal. A 246 (2003) 1.
[43] R. Villa, C. Cristiani, G. Groppi, L. Lietti, P. Forzatti, U. Cornaro, S. Rossini, J. Mol. Catal. A: Chem. 204–205 (2003) 637.
[44] A. Heinzel, B. Vogel, P. Hübner, J. Power Sources 105 (2002) 202.
[45] S.H.D. Lee, D.V. Applegate, S. Ahmed, S.G. Calderone, T.L. Harvey, Int. J. Hydrogen Energy 30 (2005) 829.
[46] W.J.M. Vermeiren, E. Blomsma, P.A. Jacobs, Catal. Today 13 (1992) 427.
[47] J.K. Hochmuth, Appl. Catal. B 1 (1992) 89.
[48] R. Horn, K.A. Williams, N.J. Degenstein, A. Bitsch-Larsen, D. Dalle Nogare, S.A. Tupy, L.D. Schmidt, J. Catal. 249 (2007) 380.
[49] L. Giani, G. Groppi, E. Tronconi, Ind. Eng. Chem. Res. 44 (2005) 4993.
[50] P. Ciambelli, V. Palma, E. Palo, P. Villa, Italian Patent Application SA2008A/000023.
[51] K.L. Hohn, L.D. Schmidt, Appl. Catal. A 211 (2001) 53.